J Mater Sci: Mater Med (2008) 19:3489–3495
DOI 10.1007/s10856-008-3527-x

Fabrication of porous titanium scaffold materials by a fugitive filler method

T. F. Hong · Z. X. Guo · R. Yang

Received: 16 January 2008 / Accepted: 25 June 2008 / Published online: 15 July 2008

Abstract A clean powder metallurgy route was developed here to produce Ti foams, using a fugitive polymeric filler, polypropylene carbonate (PPC), to create porosities in a metal-polymer compact at the pre-processing stage. The as-produced foams were studied by scanning electron microscopy (SEM), LECO combustion analyses and X-ray diffraction (XRD). Compression tests were performed to assess their mechanical properties. The results show that titanium foams with open pores can be successfully produced by the method. The compressive strength and modulus of the foams decrease with an increasing level of porosity and can be tailored to those of the human bones. After alkali treatment and soaking in a simulated body fluid (SBF) for 3 days, a thin apatite layer was formed along the Ti foam surfaces, which provides favourable bioactive conditions for bone bonding and growth.

1 Introduction

Biomaterials for tissue engineering must be highly biocompatible so as to avoid prolonged inflammatory response, immunogenicity or cytotoxicity. An ideal bone scaffold material must also display a wide range of properties and characteristics in order to augment de novo bone formation. The structure must be highly porous with interconnected pores in the size range of 50–500 μm [1, 2], which provides sufficient space for cell ingrowth, attachment and proliferation to form newly generated bone tissues, and also for the transport of body fluids with essential nutrients to the site [3–6].

Various materials have been developed for tissue engineering of bone or cartilage, including ceramics (e.g., hydroxyapatite (HA), and tricalcium phosphate (TCP)), bioglass, and polymers (e.g., poly(L-lactide) (PLLA), polyglycolic acid (PGA), collagen and chitin) [2, 7–11]. These porous bioactive ceramic and polymeric scaffolds promote bone or tissue growth into the open pores, thereby allowing a rapid return of the repaired body part to the physiologically acceptable state of function. However, the porous ceramic and polymeric scaffold materials show poor mechanical properties. The porous ceramics are usually very brittle and prone to fracture upon sudden impact, particularly during the healing stage. Porous polymers are often of much lower strength than human bones. Therefore, it is desirable to develop scaffold implant materials with both reliable mechanical properties and porous structures, similar or superior to natural bones.

Metallic materials have been widely applied in orthopaedics for a long time, especially for high load-bearing applications, such as dental, maxillofacial, spinal, femur and knee joints, and bone plate and screws. Ti and its alloys are of particular interest because of their relative low density, high strength-to-elastic modulus ratio, outstanding corrosion resistance and good biocompatibility [12–14]. However, due to its high melting point (1,670°C), and high chemical affinity with atmospheric gases (oxygen and nitrogen) and most mould materials, it is difficult to

T. F. Hong
Department of Materials Engineering, National Pingtung University of Science and Technology, Pingtung 91201, Taiwan
e-mail: tfhong@mail.npust.edu.tw

Z. X. Guo (✉)
Department of Chemistry, University Colloge London, London WC1H 0AJ, UK
e-mail: z.x.guo@ucl.ac.uk

R. Yang
Institute of Metal Research, Chinese Academy of Sciences, Shenyang 110016, China

synthesise titanium foams by a solidification process. Powder metallurgy techniques provide desirable pathways of synthesising porous Ti structures under relatively low temperatures with low reactivity [6, 15–22]. In addition, implant surfaces play a key role in biocompatibility. Recently, there has been an increasing interest in using simple chemical and biomineralisation methods to treat and bioactivate Ti surfaces at a relative low temperature [23–29], especially for samples with a complex shape or porous structure.

Here, a clean powder metallurgy route was developed using polypropylene carbonate (PPC) granules as fugitive fillers in a Ti powder compact to produce titanium foams. The foam morphology and structures were studied by scanning electron microscopy (SEM). LECO combustion analyses and X-ray diffraction (XRD) were conducted to determine the level of impurities and whether there is any new crystalline phase formed after the burn-out and sintering. Their mechanical strength and modulus were determined by compression tests. After alkali and water treatment, the samples were soaked in a simulated body fluid (SBF) to induce bone-like apatites on the surfaces. The results were analysed for potential applications in bone scaffolding.

2 Experiment procedure

Pure titanium (Ti, particle size: ≤45 μm, purity: >99.0%, STREM) powder was used as a model starting material. Polypropylene carbonate ($[–CH(CH_3)CH_2OCO_2–]_n$, PPC, Mw = 50,000, Aldrich) was selected as a filler, because it can fully decompose into monomers at a relatively low temperature (<250°C) under vacuum. The as-received Ti powder is irregular and the PPC is rod-like (Fig. 1).

The PPC rods were firstly chilled in liquid nitrogen and then pulverised by a Glen Creston centrifugal mill with a sieve of 1 mm aperture. The Ti powder and filler particles were then mixed in a SPEX ball mill for 10 min with PPC volume fractions of 0, 10, 30, 50 and 60%. The mixed powders were subsequently cold compressed into a cylindrical green compact of 10.5 mm in diameter under 100 and 400 MPa, respectively.

The compacted samples were then heated at 10°C/min from room temperature to 150°C, then 1°C/min to 220°C, and finally held at 220°C for 1 h to remove the fugitive filler from the compacts. The preform was then warmed up at 5°C/min to 1,000°C and sintered in a vacuum furnace under 1×10^{-4} torr (1.3×10^{-3} Pa) for a designated period of time (2.5, 5 or 10 h) before being furnace cooled to ambient temperature. Scanning electron microscopy was used to characterise the cell morphology of the sintered foams. To assess possible contamination involved from the processing, LECO combustion techniques were used to analyse the impurities in the sintered samples. Compression tests were performed on the specimens with a constant cross-head velocity of 1 mm/min.

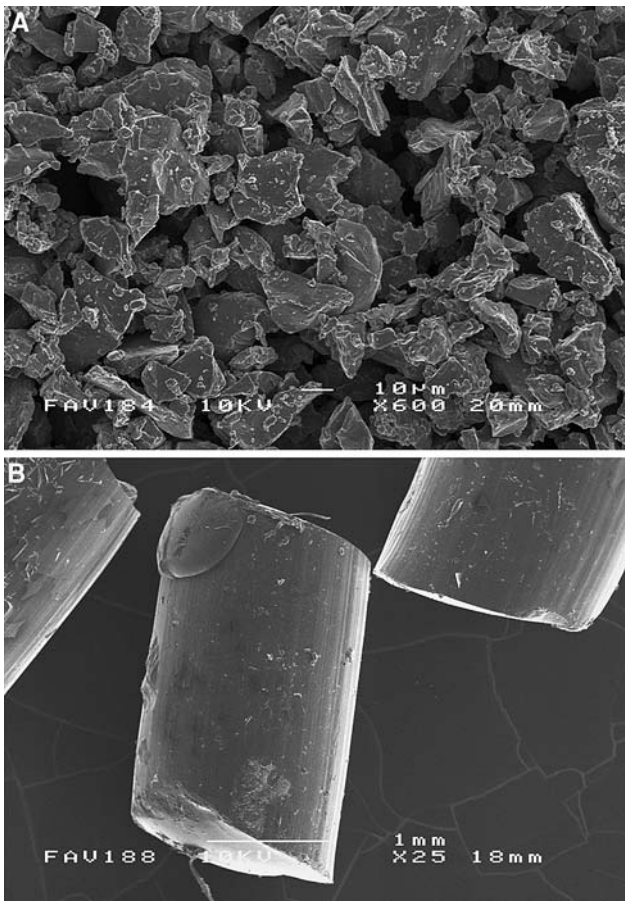

Fig. 1 SEM images of as-received materials: (**a**) Ti and (**b**) PPC

Selected porous Ti samples were sliced into plates of 1 mm thickness and ultrasonically cleaned in acetone, ethanol and pure water for 15 min each to remove possible impurities introduced during sectioning, and then immersed in a 5 M NaOH aqueous solution at 60°C for 24 h. After the alkali treatment, the samples were then immersed in deionised water at 60°C for 24 h. All the treated Ti samples were soaked in a 1.5 m-SBF at 36.5°C up to 3 days for biomimetic apatite coating. The 1.5 m-SBF was prepared by dissolving NaCl, $NaHCO_3$, Na_2CO_3, KCl, $K_2HPO_4 \cdot 3H_2O$, $MgCl_2 \cdot 6H_2O$, 0.2 M NaOH, HEPES, $CaCl_2$ and Na_2SO_4 in deionised water and buffered to PH 7.4 at 36.5°C by 1.0 M NaOH, and the ion concentrations were 1.5 times the standard m-SBF (Na^+ 142.0, K^+ 5.0, Mg^{2+} 1.5, Ca^{2+} 2.5, Cl^- 103.0, HCO_3^- 10.0, HPO_4^{2-} 1.0, and SO_4^{2-} 0.5 mM^{-1}) [30]. The samples were then carefully washed with pure water, and dried in an oven at 40°C for 24 h.

Surface morphology of the Ti samples was examined by field emission scanning electron microscopy (FE-SEM, JEOL JSM 6300F). The surfaces of the samples were analysed by energy dispersive X-ray spectroscopy (EDX, INCA X-stream Module), and X-ray diffractometry (XRD, Simens D-5000). The XRD was performed at 2θ angles from 20 to 60° at a scanning speed of 0.6°/min.

3 Results and discussion

After being chilled by liquid nitrogen and then milled in a centrifugal device with a 1 mm aperture sieve, PPC rods were mainly pulverised into particles of 100–600 μm (Fig. 2a). Moreover, the milled PPC fillers were well distributed among Ti starting particles after 10-min mixing in a SPEX shaker mill, where the Ti particles were evenly coated on the surfaces of PPC (Fig. 2b). Therefore, the process is effective in producing Ti powder coated filler, ideal for generating porous structures with well-distributed pores and uniform cell walls after burn-out and sintering.

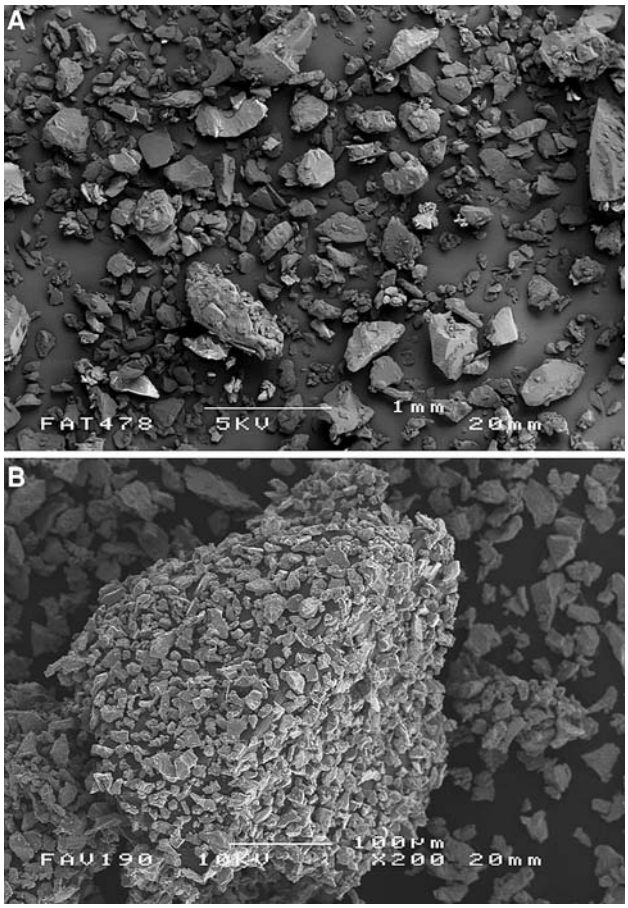

Fig. 2 SEM images of milled powder: (**a**) PPC and (**b**) Ti with PPC

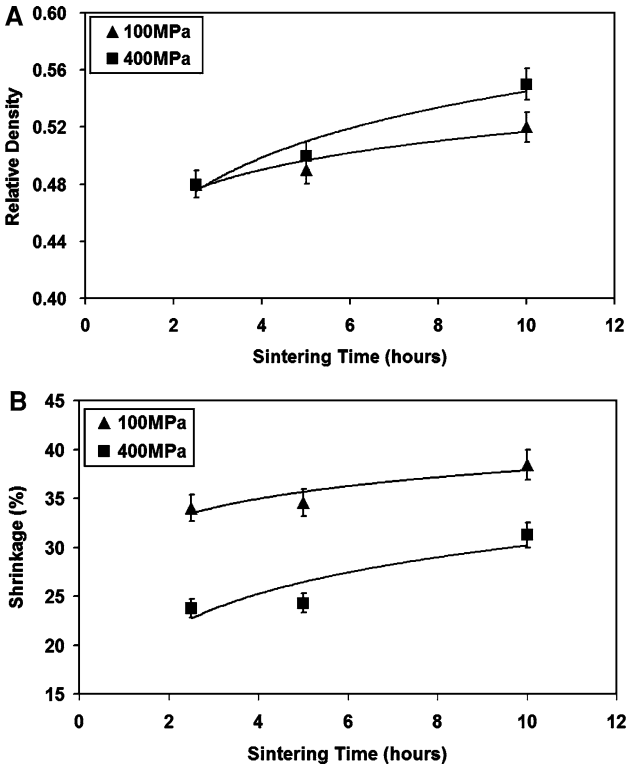

Fig. 3 Geometric variation with sintering time of a Ti-50PPC porous material, cold-compacted under 100 and 400 MPa, respectively: (**a**) relative density versus sintering time and (**b**) shrinkage versus sintering time

The burn-out conditions were selected according to previously optimised parameters in the laboratory [31].

The effect of sintering time on the geometry variations of the Ti-50PPC samples are shown in Fig. 3. Figure 3a depicts the relationship between the sintering time and the relative density (apparent density/theoretical density) of the Ti-50PPC samples, where the relative density increases with sintering time in both cases. Moreover, the difference between the relative densities also indicates that the cold compaction pressure affect the density. The 400 MPa curve shows a steeper slope than the 100 MPa curve, and the gap between the two curves becomes greater with increasing sintering time. The higher cold compaction load produced denser green compacts or closer powder-powder contacts, and therefore speeds up the sintering process via diffusion. This is further confirmed by the relationship between the sintering time and shrinkage of the Ti-50PPC samples (Fig. 3b). As the samples pressed under 400 MPa are more compact than those pressed under 100 MPa, there is less shrinkage in the former during sintering. However, the higher cold compact pressure leads to greater sintering kinetics, as noted by the steeper slope in the densification curve.

Figure 4 shows SEM images of a Ti-50PPC foam cold-pressed under 100 MPa and sintered at 1,000°C for 5 h. It

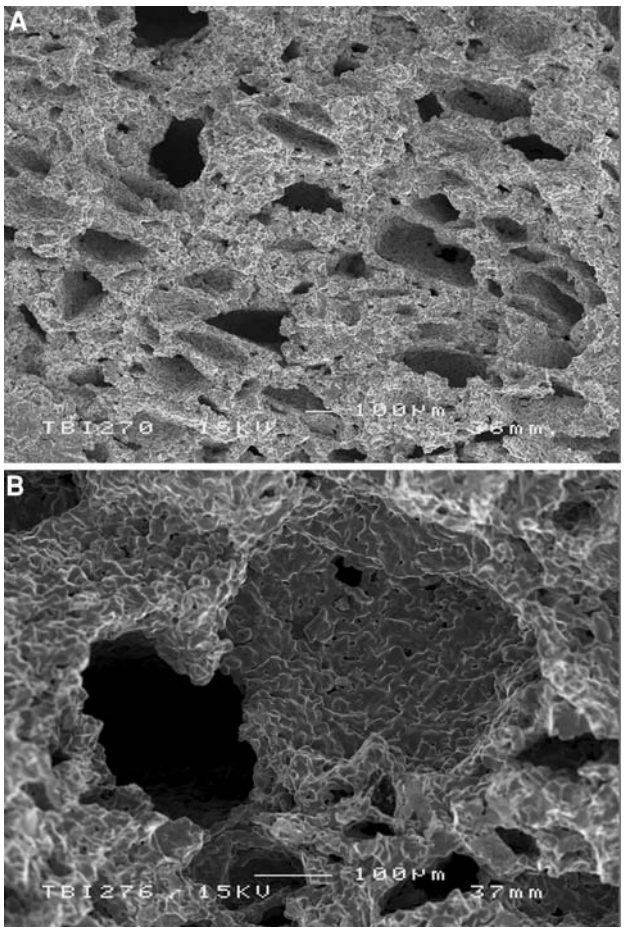

Fig. 4 SEM images of a Ti foam structure (Ti-50PPC): (**a**) interconnected cells and (**b**) window and meso-pores in cell walls

is clear that the cells are open (Fig. 4a), and interconnected by pores or "windows" of tens of microns (Fig. 4b). The windows provide pathways for body fluid and nutrient transportation, essential for bone regeneration and growth. The cell walls are also porous with meso-pores of a few microns, which are also beneficial to osteoblasts attachment [32], and may enhance osteoconductivity in bone scaffold applications.

XRD was used to check whether there is any new crystalline phase formed after burn-out and sintering. Figure 5 compared the X-ray diffraction patterns of the as-received Ti powder (A); the Ti-50PPC samples sintered at 1,000°C for 2.5 h (B) and 10 h (C), respectively. Clearly, no additional crystalline phase was found after the treatments. Possible impurities of carbon and oxygen in the as-received Ti, sintered Ti, and sintered Ti-50PPC samples were measured by LECO combustion techniques. The results are compared in Table 1 and suggest that some impurities were introduced from the sintering process. The PPC filler contributed some carbon and oxygen to the samples.

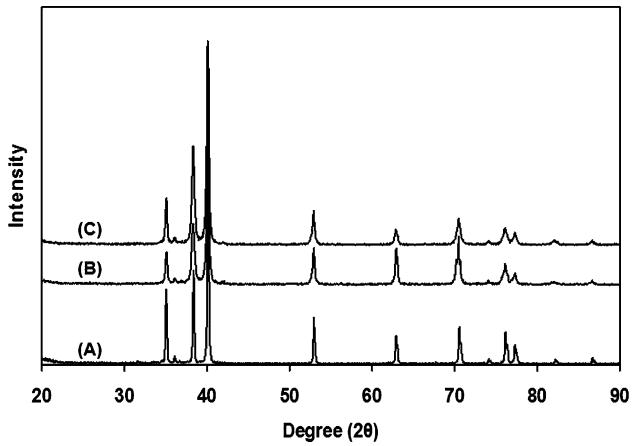

Fig. 5 XRD patterns of different Ti samples: (**a**) as-received Ti powder; (**b**) Ti-50PPC sintered at 1,000°C for 2.5 h; and (**c**) Ti-50PPC sintered at 1,000°C for 10 h

Table 1 Carbon and oxygen contents in Ti samples by LECO analyses

Sample	Carbon content (wt%)	Oxygen content (wt%)
As-received Ti	0.02	0.03
Ti (1,000°C, 10 h)	0.06	0.49
Ti-50PPC (1,000°C, 10 h)	0.17	0.66

The mechanical properties of the sintered foams were evaluated by compression tests. Figure 6a shows the relationship between the compressive strength and the relative density of the sintered Ti foams. The samples were all cold compressed under 100 or 400 MPa and sintered at 1,000°C for 2.5, 5, and 10 h, respectively. In general, the longer the sintering time, the higher the relative density and the greater the compressive strength of the sample. Moreover, the samples cold-pressed under 400 MPa possess a relatively high density and compressive strength. This is because the higher cold compaction increases the contact of particles, and hence gives faster densification kinetics during sintering. However, as the relative density increases, both the strength and modulus seem to increase slightly faster for the 100 MPa compressed samples than for the 400 MPa compressed ones. The intersection point seems to be around a foam density of 0.5. The switch-over in the properties is likely due to enhanced particle-particle bonding after prolonged sintering to achieve the same density for the 100 MPa compressed sample.

The similar result can also be found in Young's modulus-relative density relationship in Fig. 6B. The Young's modulus and relative density are all increased with the increase of sintering time. Overall, the 400 MPa compressed sample has higher relative density and modulus

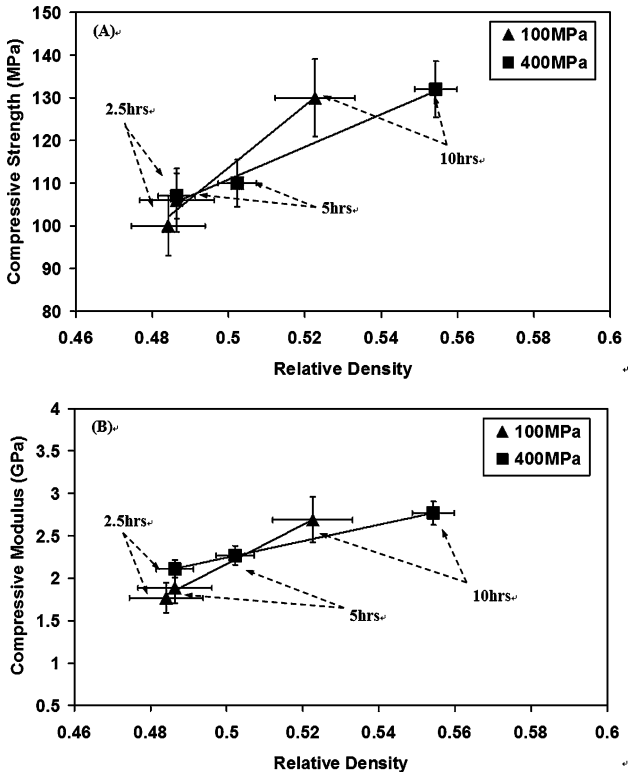

Fig. 6 Ti-50PPC isothermal curves under different cold compression and sintering conditions: (**a**) compressive strength versus relative density and (**b**) compressive modulus versus relative density

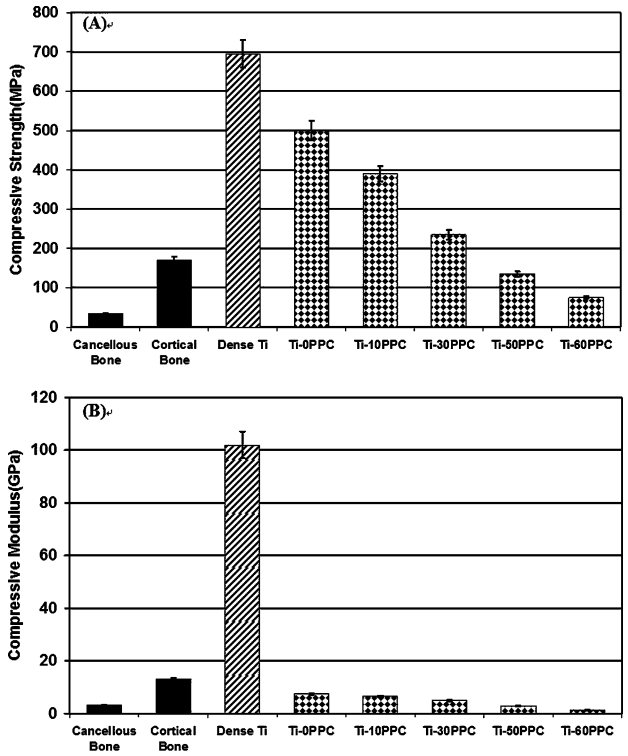

Fig. 7 Compressive mechanical properties of human bones, dense and porous Ti: (**a**) compressive strength and (**b**) compressive modulus

performance than the sample cold-pressed at 100 MPa when they were sintered under the same condition, whereas 100 MPa curve has a steeper slope than 400 MPa curve. At the shorter sintering range, the sample with 400 MPa cold compression has a higher modulus at the same relative density condition, whereas 100 MPa sample has a more efficient modulus/density performance at the sintering period after the intersection.

Figure 7 compares the results from the compression tests of a range of foams, with the values of typical bone structures obtained from Ref. [33]. It is clear that the compressive strength and modulus decrease with increasing porosity of the foams. Compared with the mechanical properties of human bones, the graphs show that the mechanical properties of 0–30% PPC samples are close to the cortical bone, whereas the properties of other structures with a higher porosity are close to the human cancellous bone. To achieve a functionally satisfactory implant for practical applications, porous scaffold design needs to consider both strength and modulus. High strength and a compatible modulus to the bone are essential for the selection of implant materials. If the modulus of a scaffold material is compatible to the replaced bone; it may stimulate bone growth and maintain a healthy bone structure to avoid bone resorption and necrosis. The mechanical properties of the foams can be tailored from foam structures for the design and selection of required implant materials.

The surface structural and chemical characterisations after bioactivation treatment are shown in the SEM images and EDX results of the relevant Ti samples, respectively. From the SEM images (Fig. 8), it is noted that a submicron-sized porous network structure was formed after the NaOH treatment, and the pores were apparently more open after the water treatment. It is clear that depositions have covered the porous structure after soaking in the 1.5 m-SBF for 1 day and a layer of coating was formed after immersion for 3 days in the 1.5 m-SBF. The EDX analysis (Fig. 9) reveals that the Na concentration decreased dramatically after immersion in deionised water at 60°C for 24 h. Ca and P were detected in the samples soaked in 1.5 m-SBF for 1 day, and their intensity increased after immersion for 3 days in the 1.5 m-SBF. A certain level of crystallinity in the apatite structure may have been developed in the sample.

Submicron pore sizes and negatively charged titania surfaces were required to assist apatite nucleation [34]. An amorphous sodium titanate hydrogel layer was formed on the Ti surface after the NaOH treatment. After sodium ions were released from the sodium titanate layer by the water

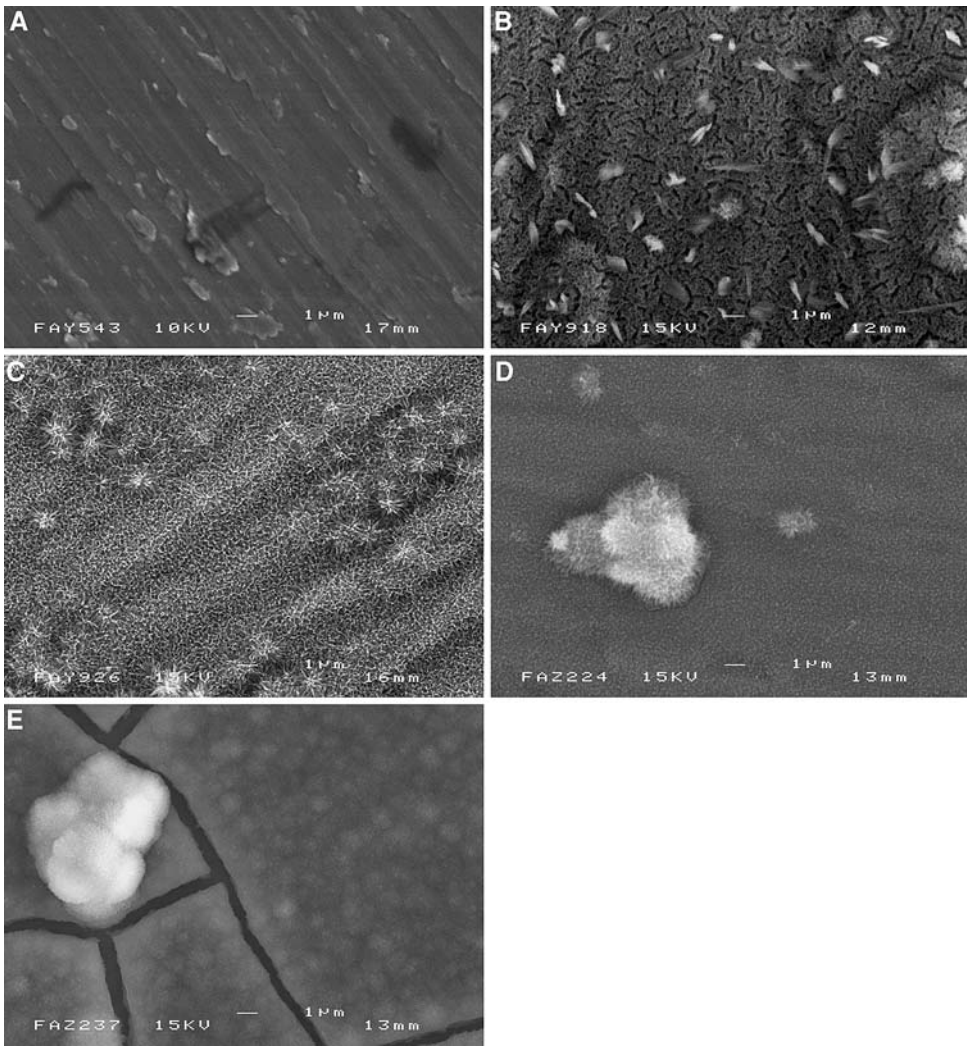

Fig. 8 SEM images of Ti surfaces: (**a**) as-cleaned Ti, (**b**) after NaOH treatment, (**c**) after NaOH + water treatment, (**d**) in 1.5 m-SBF 1 day, and (**e**) in 1.5 m-SBF 3 days

treatment, the Ti–OH groups based upon the anatase structure have a specific structural arrangement effective for inducing apatite nucleation [35]. The Ti–OH groups initially combined with calcium ions in the SBF to form positively charged amorphous calcium titanate. This layer attracted negatively charged phosphate ions in the SBF to form amorphous calcium phosphate and eventually transformed into crystalline apatite [29]. The 1.5 m-SBF has higher ion concentrations than the m-SBF, therefore, speeding up the apatite nucleation on the surfaces of Ti samples. The apatite layer was formed only within 3 days in the 1.5 m-SBF, which is far more efficient than using the SBF [25, 35]. After implantation, living tissues are expected to bond with the formed apatite layer biochemically and grow into the porous structure to provide mechanical interlocking and healthy nutrient circulation. Further in vitro tests are required to confirm such beneficial effects, which are beyond the scope of the present paper.

4 Conclusions

A clean powder metallurgy route was successfully developed to produce porous open-cellular Ti structures for medical scaffold and maxillofacial applications. The cell size and shape of the foam structures can be controlled by the PPC filler and Ti particle sizes. The as-produced Ti foams are characterised by interconnected pores with 10–60% porosity and pore sizes mainly between 50 and 500 μm. The compressive strength and modulus of the foams decrease with an increasing level of porosity and can be tailored to those of the human bones. The surface of the Ti foams can be readily bioactivated by simple alkali and water treatment. The fine micron-level porous surface structure produced from the treatments provided excellent apatite nucleation sites in the 1.5 m-SBF. Further biological compatibility tests may be carried out to investigate their potentials as a new generation of implant materials for bone tissue engineering.

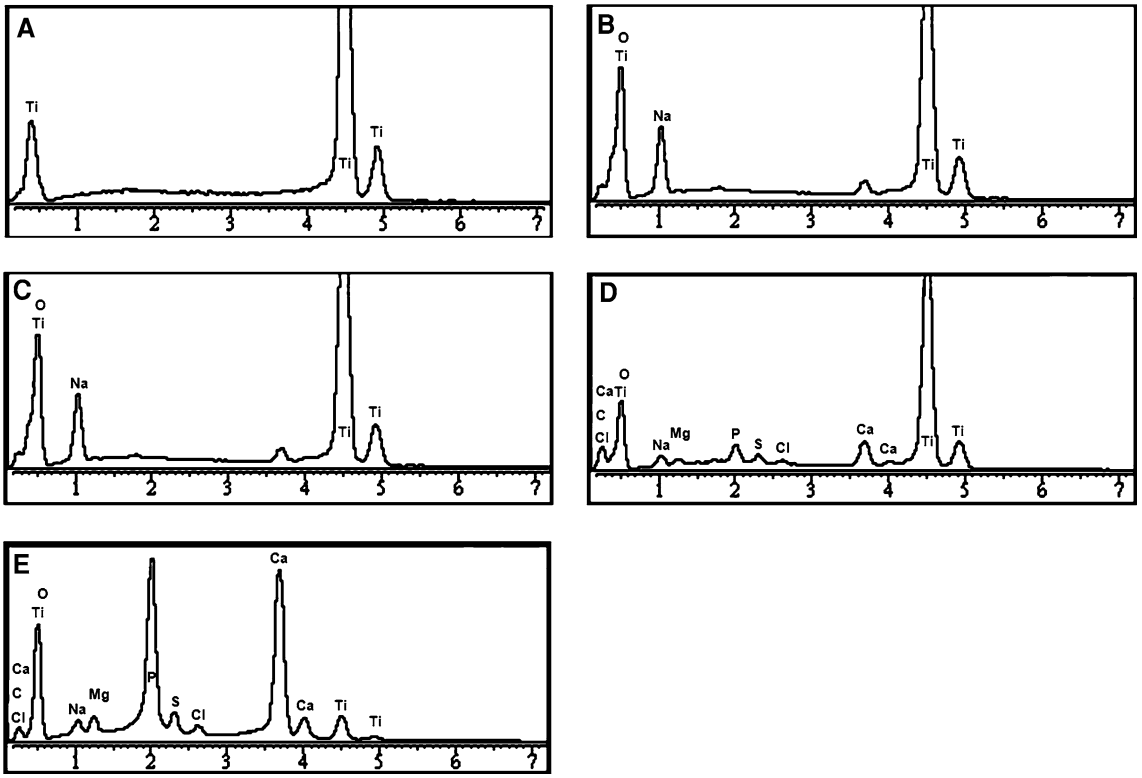

Fig. 9 EDX analysis of Ti surfaces: (**a**) as-cleaned Ti, (**b**) after NaOH treatment, (**c**) after NaOH + water treatment, (**d**) in 1.5 m-SBF 1 day, and (**e**) in 1.5 m-SBF 3 days

References

1. G. Ryan, A. Pandit, D.P. Apatsidis, Biomaterials **27**, 2651 (2006)
2. S.J. Simske, R.A. Ayers, T.A. Bateman, Mater. Sci. Forum **250**, 151 (1997)
3. C.E. Wen, Y. Yamada, K. Shimojima, Y. Chino, H. Hosokawa, M. Mabuchi, J. Biomed. Mater. Res. **17**, 2633 (2002)
4. L.D. Zardiackas, D.E. Parsell, L.D. Dillon, D.W. Mitchell, L.A. Nunnery, R. Poggie, J. Biomed. Mater. Res. **58**, 180 (2001)
5. T.M. Freyman, I.V. Yannas, L.J. Gibson, Prog. Mater. Sci. **46**, 273 (2001)
6. C.E. Wen, M. Mabuchi, Y. Yamada, K. Shimojima, Y. Chino, T. Asahina, Scripta Mater. **45**, 1147 (2001)
7. Y. Zhang, H.H.K. Xu, S. Takagi, J. Mater. Sci. Mater. Med. **17**, 437 (2006)
8. D.W. Hutmacher, Biomaterials **21**, 2529 (2000)
9. X. Liu, P.X. Ma, Ann. Biomed. Eng. **32**, 477 (2004)
10. H. Yoshikawa, A. Myoui, J. Artif. Organs **8**, 131 (2005)
11. M. Kellomaki, H. Niiranen, K. Puumanen, N. Ashammakhi, T. Waris, P. Tormala, Biomaterials **21**, 2495 (2000)
12. D. Kuroda, M. Niinomi, M. Morinaga, Y. Kato, T. Yashiro, Mater. Sci. Eng. **A243**, 244 (1998)
13. W.F. Ho, C.P. Ju, C.H. Chern Lin, Biomaterials **20**, 2115 (1999)
14. D. M. Brunette, P. Tengvall, M. Textor, P. Thomsen, *Titanium in Medicine* (Springer-Verlag, Berlin, 2001)
15. D.C. Dunand, Adv. Eng. Mater. **6**, 369 (2004)
16. J. Banhart, Prog. Mater. Sci. **46**, 559 (2001)
17. R. Ricceri, F. Arcuri, P. Matteazzi, J. Phys. IV **11**, 51 (2001)
18. R. Ricceri, P. Matteazzi, Int. J. Powder Metall. **39**, 53 (2003)
19. J.P. Li, S.H. Li, K. de Groot, P. Layrolle, Key Eng. Mater. **218–220**, 51 (2002)
20. C.S.Y. Jee, N. Ozguven, Z.X. Guo, J.R.G. Evans, Metall. Mater. Trans. B **31B**, 1345 (2000)
21. Z.X. Guo, C.S.Y. Jee, N. Ozguven, J.R.G. Evans, Mater. Sci. Tech. **16**, 776 (2000)
22. C. M. Schwanke, L. Schaeffer, *Advanced powder technology* (Trans Tech., Zurich, 1999) p. 190
23. S. Fujibayashi, T. Nakamura, S. Nishiguchi, J. Tamura, M. Uchida, H.M. Kim, T. Kokubo, J. Biomed. Mater. Res. **56**, 562 (2001)
24. M. Wei, H.M. Kim, T. Kokubo, J.H. Evans, Mater. Sci. Eng. C **20**, 125 (2002)
25. F. Liang, L. Zhou, K. Wang, Surf. Coat. Technol. **165**, 133 (2003)
26. S. Fujibayashi, M. Neo, H.M. Kim, T. Kokubo, T. Nakamura, Biomaterials **25**, 443 (2004)
27. S.A. Hacking, E.J. Harvey, M. Tanzer, J.J. Krygier, J.D. Bobyn, J. Bone Joint Surg. **85B**, 1182 (2003)
28. M. Takemoto, S. Fujibayashi, M. Neo, J. Suzuki, T. Matsushita, T. Kokubo, T. Nakamura, Biomaterials **27**, 2682 (2006)
29. T. Kokubo, H.M. Kim, M. Kawashita, T. Nakamura, J. Mater. Sci. Mater. Med. **15**, 99 (2004)
30. A. Oyane, H.M. Kim, T. Furuya, T. Kokubo, T. Miyazaki, T. Nakamura, J. Biomed. Mater. Res. **65A**, 188 (2003)
31. N.R.F. Beeley, Development of a novel powder coated fibre pre-processing route for cost effective production of metal matrix composites. PhD Thesis, Queen Mary, University of London, London, 2002
32. K.T. Bowers, J.C. Keller, B.A. Randolph, D.G. Wick, C.M. Michaels, Int. J. Oral Maxillofac. Implants **7**, 302 (1992)
33. J. D. Currey, *Bones: Structure and Mechanics* (Princeton Univeristy Press, Princeton, 2002)
34. H.B. Wen, J.R. de Wijn, K. de Groot, J. Biomed. Mater. Res. **41**, 227 (1998)
35. M. Uchida, H.M. Kim, T. Kokubo, S. Fujibayashi, T. Nakamura, J. Biomed. Mater. Res. **63**, 522 (2002)